analytical chemistry

Article

Cite This: Anal. Chem. 2018, 90, 12503−12511

pubs.acs.org/ac

Nanoplasmonic Ruler for Measuring Separation Distance between Supported Lipid Bilayers and Oxide Surfaces

Abdul Rahim Ferhan,[†,∥] Barbora Špačková,[§,∥] Joshua A. Jackman,[†] Gamaliel J. Ma,[†] Tun Naw Sut,[†] Jiří Homola,[§] and Nam-Joon Cho*[,†,‡]

[†]School of Materials Science and Engineering, Nanyang Technological University, 50 Nanyang Avenue 639798, Singapore

[‡]School of Chemical and Biomedical Engineering, Nanyang Technological University, 62 Nanyang Drive 637459, Singapore

[§]Institute of Photonics and Electronics, Czech Academy of Science, Chaberská 57, Prague 8 18251, Czech Republic

Supporting Information

ABSTRACT: Unraveling the details of how supported lipid bilayers (SLBs) are coupled to oxide surfaces is experimentally challenging, and there is an outstanding need to develop highly surface-sensitive measurement strategies to determine SLB separation distances. Indeed, subtle variations in separation distance can be associated with significant differences in bilayer−substrate interaction energy. Herein, we report a nanoplasmonic ruler strategy to measure the absolute separation distance between SLBs and oxide surfaces. A localized surface plasmon resonance (LSPR) sensor was employed to track SLB formation onto titania- and silica-coated gold nanodisk arrays. To interpret measurement data, an analytical model relating the LSPR measurement response to bilayer−substrate separation distance was developed based on finite-difference time-domain (FDTD) simulations and theoretical calculations. The results indicate that there is a larger separation distance between SLBs and titania surfaces than silica surfaces, and the trend was consistent across three tested lipid compositions. We discuss these findings within the context of the interfacial forces underpinning bilayer−substrate interactions, and the nanoplasmonic ruler strategy provides the first direct experimental evidence comparing SLB separation distances on titania and silica surfaces.

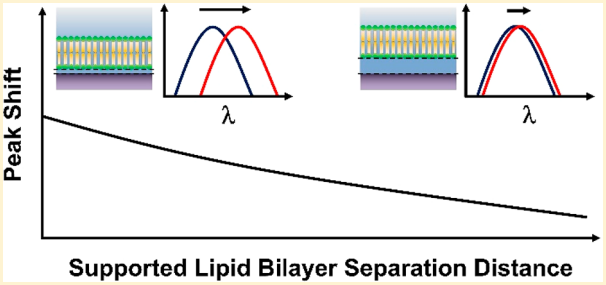

Surface-based nanoplasmonic sensors are a promising class of surface-sensitive measurement tools to probe biomacromolecular interaction processes.[1−4] When incident light interacts with metallic nanostructures, electronic excitation causes the collective oscillation of free electrons in the metal's conduction band that gives rise to one or more types of optical phenomena involving propagating and/or localized plasmon modes.[5,6] In addition to simple optical requirements and label-free reporting, a key feature of nanoplasmonic sensors is that the sensing capabilities can be tailored according to the platform design. Depending on the nanostructured architecture, light coupling to various plasmon modes occurs and the measurement responses associated with distinct modes have different degrees of surface sensitivity.[7,8]

Within this scope, localized surface plasmon resonance (LSPR) sensors based on nonperiodic arrays of metallic nanoparticles on dielectric supports have demonstrated excellent merits for highly surface-sensitive measurements in liquid environments.[9,10] LSPR generation causes an enhanced electromagnetic field in the near vicinity of metallic nanoparticles (decay length of ∼5−20 nm) and a peak in the optical extinction spectrum that is located at the surface plasmon resonance wavelength (λ_{max}).[11] The wavelength position of λ_{max} is sensitive to the local dielectric environment, and adsorption of higher refractive index biomacromolecules such as proteins and lipid vesicles typically causes a positive $\Delta\lambda_{max}$ shift.[12] These measurement capabilities are further aided by material science advances that facilitate indirect nanoplasmonic sensing,[13,14] whereby sensing platforms are coated with a thin, conformal layer of a dielectric material (e.g., silica) and detected interactions occur at the dielectric−liquid interface such that the metallic nanoparticles act as embedded plasmonic antennas.[15−17] In turn, this indirect sensing approach has opened the door to studying a wide range of biointerfacial science applications, including protein denaturation,[18] membrane−peptide interactions,[19] and supported lipid bilayer (SLB) formation on oxide film surfaces.

One of the most promising applications involves distinguishing the conformational properties of adsorbed phospholipid assemblies at solid−liquid interfaces.[20] Jonsson et al. first reported that the spontaneous rupture of adsorbed vesicles to form an SLB on a silica-coated nanohole array could be monitored on the basis that lipid molecules in an SLB configuration are, on average, closer to the sensor surface and hence in a region of higher field intensity that yields a larger

Received: May 18, 2018
Accepted: October 1, 2018
Published: October 1, 2018

DOI: 10.1021/acs.analchem.8b02222
Anal. Chem. 2018, 90, 12503−12511

measurement response.[21] Hence, the onset of SLB formation was detected by an increase in the rate of change of the corresponding measurement response. Larsson et al. validated the sensing concept with LSPR measurements by tracking vesicle rupture and SLB formation on silica-coated gold nanodisk arrays.[22] Extending this approach, it was further demonstrated that surface-sensitive LSPR measurements could be utilized to track vesicle adsorption and deformation on titania-coated gold nanodisk arrays, enabling detailed investigation of how lipid concentration,[23] vesicle size,[23] membrane phase state,[24] temperature,[24] osmotic pressure,[25] and the presence of divalent cations[25] affect vesicle adsorption kinetics. In the latter case, adsorbed vesicles typically do not rupture on titania surfaces,[26] and the sensing principle is based on measuring the extent of vesicle deformation, which is governed by the balance between membrane bending energy and vesicle−substrate interaction energy.[27,28] In particular, lipid molecules in a more deformed vesicle are, on average, in a region of higher field intensity.[29]

While the aforementioned measurement examples relied on the size mismatch between adsorbed lipid vesicles and the decay length of the enhanced electromagnetic field, experimental evidence suggests that it is also possible to detect more subtle, sub-1 nm variations in SLB proximity to silica surfaces arising from the distance-dependent field intensity and relative position of the SLB platform within the probing volume.[30] Specifically, when there is a stronger lipid−substrate interaction, the separation distance between the SLB and silica surface is smaller (tighter coupling[31]), and consequently, the lipid molecules are, on average, within a region of higher field intensity that contributes to a larger measurement response. These experimental capabilities offer competitive advantages over alternative techniques (see the Introduction in ref 30) and provide an analytical route to address outstanding questions as they relate to the coupling of SLB platforms to different solid supports. For example, SLB coupling, manifested through a combination of frictional and interfacial force components, plays an important role in modulating membrane properties such as phase behavior[32−34] and fluidity.[35,36] While empirical observation of SLB proximity sensing on silica surfaces is a compelling first step, extending this approach to comparatively measure SLB separation distance across different surfaces requires validation through experiment and simulation, and would provide a broadly useful analytical tool for SLB characterization. Indeed, it is currently understood that the efficiency of the SLB formation process depends on the strength of lipid−substrate interactions; however, it has proven experimentally challenging to determine how SLB separation distance depends on the substrate material. The development of label-free nanoplasmonic sensing strategies to quantitatively measure SLB separation distances across different sensor surfaces would provide new experimental capabilities to gain insight into SLB architectures and evaluate lipid−substrate interaction strengths.

Herein, we conducted transmission-mode LSPR experiments to measure SLB separation distances on titania- and silica-coated gold nanodisk arrays, and performed corresponding finite-difference time-domain (FDTD) simulations and theoretical calculations to guide data analysis. To facilitate these studies, a set of positively charged lipid compositions was identified that forms SLBs on both titania and silica surfaces, and it was therefore possible to measure the extent of vesicle deformation (prior to vesicle rupture) and SLB separation distance. Following this approach, it was identified that titania-supported SLBs are less tightly coupled to the sensor surface than silica-supported SLBs, and the composition-dependent variations in separation distance agreed well with the measured extent of vesicle deformation. In particular, minor variations in the lipid−substrate interaction could be detected on the basis of SLB spatial proximity, and this sensing approach facilitated the first direct experimental evidence to show that SLBs on titania surfaces have a larger separation distance than equivalent SLBs on silica surfaces. We discuss these findings in the context of the interfacial science of solid-supported phospholipid assemblies and draw out broader implications for utilizing nanoplasmonic sensors in biointerfacial science applications.

MATERIALS AND METHODS

Localized Surface Plasmon Resonance Measurements. The LSPR experiments were conducted using an Insplorion XNano instrument (Insplorion AB, Gothenburg, Sweden), which is based on an indirect nanoplasmonic sensing platform that utilizes oxide film-coated arrays of gold nanodisks, as previously described.[23] Titanium oxide and silicon nitride were used as base materials for the conformal coatings on the titania- and silica-coated arrays, respectively. For the silica-coated arrays, a thin silicon oxide overlayer was formed through the oxidation of silicon nitride upon exposure to oxygen plasma.[37] To ensure consistency across different measurement runs, all sensor chips used in this work were from the same fabrication batch and the number of repeated usages for each sensor chip was limited to two times (for repeat measurements). Immediately prior to each measurement, the sensor was successively rinsed with a solution of 1% sodium dodecyl sulfate (SDS) in water, water, and ethanol, dried under a stream of nitrogen gas, and treated with oxygen plasma for 1 min (Harrick Plasma, Ithaca, NY, U.S.A.). The same rinsing procedure was applied in between repeat measurements, as previously described.[38] A peristaltic pump (Reglo Digital, Ismatec, Glattburg, Switzerland) was used to inject liquid samples, including aqueous solutions containing lipid vesicles with varying molar ratios of 1,2-dioleoyl-*sn*-glycero-3-phosphocholine (DOPC) and 1,2-dioleoyl-*sn*-glycero-3-ethylphosphocholine (DOEPC) lipids, at a flow rate of 100 μL/min. The LSPR peak wavelength (denoted as λ_{max}) in the optical extinction spectrum was determined by high-order polynomial fitting.[39] The measurement data were collected with a time resolution of 1 Hz, and data analysis was performed using the Insplorer software package (Insplorion AB).

Finite-Difference Time-Domain Simulations. The FDTD simulations were performed using the Lumerical FDTD Solutions software package (Vancouver, BC, Canada). The simulated structure consisted of a tapered gold nanodisk with rounded edges, which was located on a glass substrate and surrounded by a liquid medium (aqueous buffer). The entire structure was covered with a 10 nm thick sputtered oxide layer. The refractive index (RI) values of the titania and silica coats were determined by ellipsometric measurements that were performed using equivalently prepared glass substrates without nanodisks. The RI values at 700 nm wavelength were determined to be 2.32 and 1.97 for the titania- and silica-coated substrates, respectively (see the Supporting Information of ref 29). Of note, the apparent RI value for the silica-coated substrate is higher than typical RI values for silica due to the use of silicon nitride as the base material for the conformal

DOI: 10.1021/acs.analchem.8b02222
Anal. Chem. 2018, 90, 12503−12511

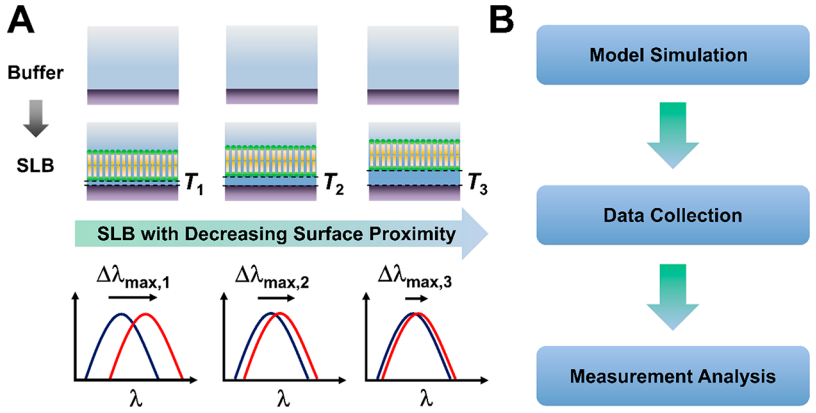

Figure 1. (A) Schematic illustration of the nanoplasmonic ruler concept relating the LSPR measurement response to SLB separation distance on the sensor surface. (B) Overview of the measurement strategy; model simulation of SLB separation distance on different sensor surfaces provides the basis for data interpretation and measurement analysis.

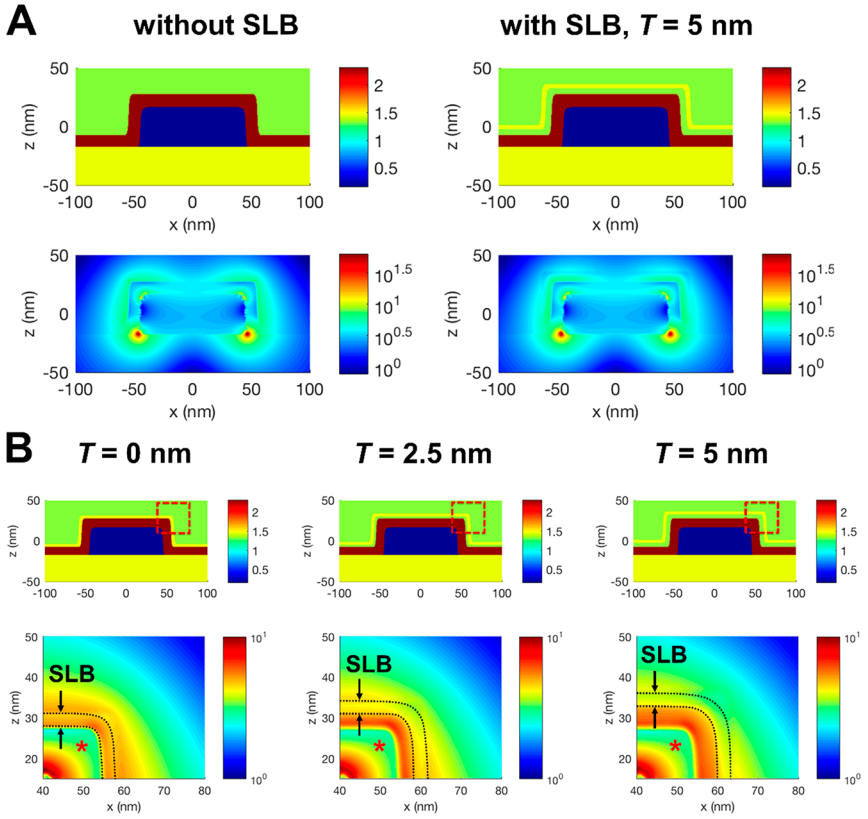

Figure 2. (A) Cross-sectional distribution of the refractive index (real part) for an individual, titania-coated gold nanodisk in aqueous buffer environment (top) and corresponding FDTD simulations of the electric field distribution in the same space (bottom). The data are presented for nanodisks without (left) and with (right) SLB coatings at a separation distance of 5 nm. (B) Equivalent refractive index distributions are presented for nanodisks with SLB coatings at a separation distance of 0, 2.5, or 5 nm, respectively (top). The red dashed boxes indicate the regions in which corresponding FDTD simulations are presented in magnified view (bottom). In the FDTD simulations, the asterisks indicate the location of the dielectric coating, while the arrows and dashed lines define the boundaries of the SLB coating.

coating. The dielectric constant of gold was taken from ref 40, and the RI of the glass substrate and buffer were set at 1.45 and 1.336, respectively. The shape and dimensions of the nanodisk were optimized to fit the experimentally measured extinction peak positions of both silica- and titania-coated substrates immersed in solutions with refractive indexes ranging from 1.335 to 1.384 RIU. The best fit was obtained for the nanodisk with a bottom diameter of 95 nm, a top diameter of 85 nm, and a height of 35 nm, with rounded edges. A grid size of 0.5 nm was used for the simulations.

RESULTS AND DISCUSSION

Indirect Nanoplasmonic Sensing Approach. Our measurement scheme utilizes a dielectric-coated gold nanodisk array as the sensing platform. Briefly, noninteracting and nonperiodic arrangements of plasmonic gold nanodisks (~100 and ~20 nm in diameter and height, respectively) were fabricated on a glass substrate by hole−mask colloidal lithography.[41] Then, the entire sensing surface was sputter-coated with a thin, conformal layer of titania or silica dielectric

DOI: 10.1021/acs.analchem.8b02222
Anal. Chem. 2018, 90, 12503−12511

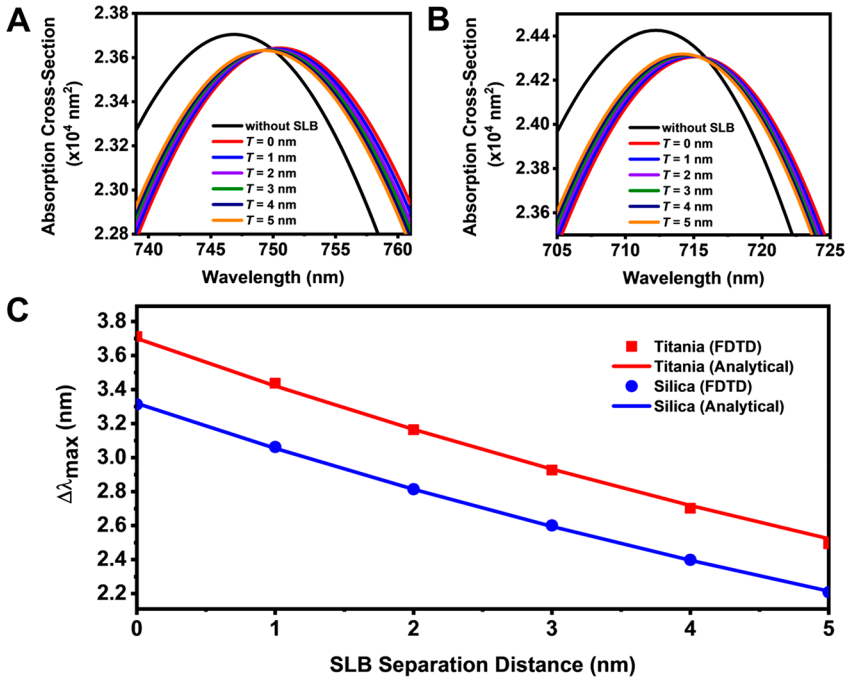

Figure 3. LSPR extinction spectra of the simulated nanodisk structure without and with SLB coatings for (A) titania- and (B) silica-coated sensor surfaces. The SLB separation distance was varied between 0 and 5 nm. (C) Plot of the relationship between LSPR peak shift ($\Delta\lambda_{max}$) and SLB separation distance for titania- and silica-coated sensor surfaces based on FDTD simulations and analytical calculations.

material (~10 nm thick coating). In this configuration, the embedded gold nanodisks act as plasmonic antennas and part of the enhanced electromagnetic field extends beyond the dielectric coating.[22] Upon light illumination, the gold nanodisks absorb and scatter near-visible light, as signified by a λ_{max} peak position in the far-field extinction (transmission) spectrum.[42] Depending on the material properties of the dielectric coating, the baseline λ_{max} peak position changes according to the resonance condition,[7,43−45] and the surface sensitivity of titania- and silica-coated nanodisk arrays varies accordingly.

When phospholipid molecules adsorb onto the sensor surface, a positive $\Delta\lambda_{max}$ shift occurs due to the change in the local dielectric environment. Specifically, it is the change in the λ_{max} peak position from one state (sensor surface in aqueous buffer solution) to another state (sensor surface with adsorbed lipid molecules in aqueous buffer solution). The magnitude of the $\Delta\lambda_{max}$ shift depends on the number and location of adsorbed phospholipid molecules within the probing volume. Within an SLB, the number of phospholipid molecules per unit surface area depends on the molecular packing density and hence is a fixed value for a certain type of phospholipid. Therefore, variations in the $\Delta\lambda_{max}$ shift for an SLB can be attributed to its spatial proximity to the sensor surface (Figure 1). Considering the subtle differences in $\Delta\lambda_{max}$ shifts that are recorded during spatial proximity measurements, it is important to account for the substrate-specific variations in surface sensitivity and to construct appropriate models to validate the LSPR measurement responses. This step provides the basis for comparing measurement responses across different sensor surfaces.

Simulation of SLB Separation Distance. To understand how SLB separation distance affects LSPR measurement responses, we performed FDTD simulations on titania- and silica-coated nanodisk arrays, without and with conformal SLB coatings. In the simulations, we assumed the formation of a conformal SLB across oxide-coated nanodisk arrays and the SLB was separated from the oxide film surface by a hydration layer of thickness T (Figure 2A). The thickness[46,47] (D) and refractive index[48] (n_L) of the SLB coating were defined to be 3.7 nm and 1.46, respectively, which correspond to a DOPC lipid bilayer that is representative of the SLBs used in our experiments. Of particular relevance, the value of T (the "separation distance") was varied from 0 to 5 nm in order to represent SLB platforms with varying spatial proximities to the sensor surface. This range is in line with reported estimates[49,50] of the bilayer−substrate separation distance of around 0.5−1 nm for zwitterionic SLBs on silica as a reference point. It should also be emphasized that the LSPR sensing scheme is insensitive to the hydration layer itself, and spatial proximity sensing arises from the relative location of the SLB platform within the enhanced electromagnetic field.

Following this approach, the profile of the total electric field intensity at resonance was calculated for titania- and silica-coated nanodisks without and with SLB coatings (T = 0, 2.5, 5 nm) (Figure 2B). The electric field is enhanced at the boundary of a gold nanodisk and decays into the surrounding medium; the enhancement is highest at the sharp edges of the nanodisk corners (hot spots). Due to the presence of multiple dielectric coatings, the field does not decay monotonically, as is typical for plain plasmonic nanoparticles, but rather shows complex behavior. A sharp increase in the field intensity can be seen at the interfaces between the dielectric coating and SLB and between the SLB and buffer, as the field decays from an area with higher RI to an area with lower RI.[51] Additionally, the distribution of the field on top of the dielectric coating is more uniform since the field in the areas with higher enhancement (hot spots) decays more rapidly than the field in the areas with lower enhancement, and the dielectric coating is sufficiently thick to smoothen these differences.

DOI: 10.1021/acs.analchem.8b02222
Anal. Chem. 2018, 90, 12503−12511

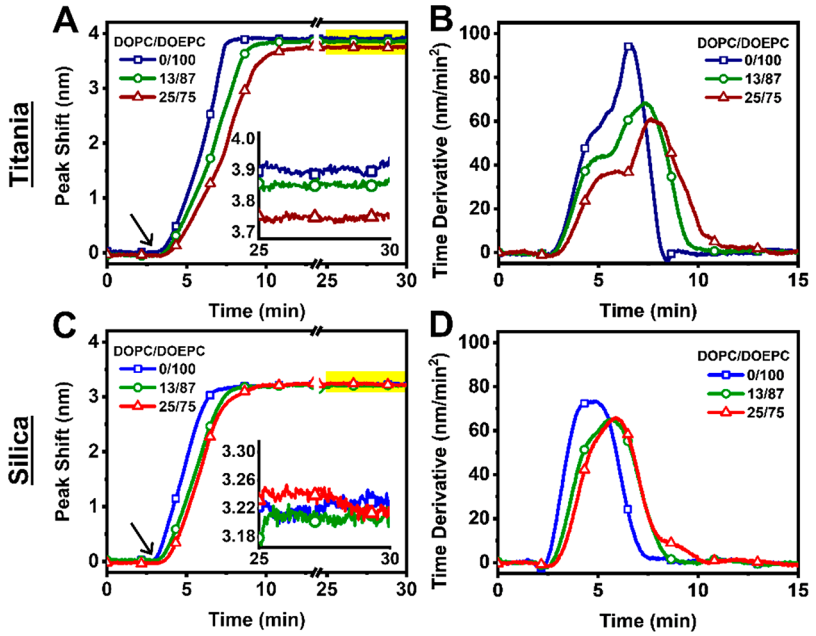

Figure 4. (A) LSPR measurement responses reporting time-resolved peak shifts for SLB formation on titania-coated gold nanodisk arrays by the vesicle fusion approach. The tested lipid compositions were 0/100, 13/87, and 25/75 mol % DOPC/DOEPC. Arrows indicate when lipid vesicles were added. The inset shows final measurement responses corresponding to the yellow highlighted region. (B) Corresponding rates of change (time derivative) in the LSPR peak shifts shown in panel A, and the data were normalized according to vesicle size. (C and D) Equivalent data are presented for SLB formation on silica-coated gold nanodisk arrays.

The simulated extinction spectra show λ_{max} peak positions at ~748 and ~716 nm for titania- and silica-coated nanodisk arrays, respectively (Figure 3, parts A and B). An SLB coating increases the λ_{max} position by several nanometer units, and the magnitude of the $\Delta\lambda_{max}$ shift is larger for SLBs that are closer to the sensor surface (smaller T). The $\Delta\lambda_{max}$ shifts as a function of SLB separation distance (as indicated by T) are presented in Figure 3C. As the separation distance decreased from 5 to 0 nm (tighter coupling), the $\Delta\lambda_{max}$ shifts increased by around 45% on each substrate and were in the range of 2−4 nm shifts, which are >250 times greater than the sensor resolution. Furthermore, the magnitudes of the $\Delta\lambda_{max}$ shifts at specific T values were larger on titania-coated surfaces, reflecting its higher surface sensitivity (as indicated in part by its higher bulk refractive index sensitivity).

The trend in simulated $\Delta\lambda_{max}$ shifts can be described analytically. We assumed that the spatial sensitivity is proportional to the distribution of the electric field ($|\mathbf{E}|^2$) and that, despite rather complex behavior, the electric field decreases from the interface between the dielectric coating and the surrounding medium proportionally to $1/(r + R_*)^6$ (refs 23, 24, 29), where r is the coordinate perpendicular to the surface of the dielectric coating (r = 0 corresponds to the interface between the dielectric coating and surrounding medium) and R_* is the length scale characterizing the distance between the center and the edge of a nanoparticle. R_* is expected to be comparable to the average distance between the nanodisk center and the interface between the dielectric coating and surrounding medium, but it has to be noted that it is also dependent on the characteristics of the structure (e.g., the nanoparticle shape, as well as the refractive indexes and thicknesses of the dielectric coating and SLB) and has to be calculated numerically. Thus, a $\Delta\lambda_{max}$ shift occurring within a layer of fixed thickness D, refractive index n_L, and distance T from the sensor interface can be expressed as

$$\Delta\lambda_{max} = S_B \Delta n \int_T^{D+T} \frac{5{R_*}^5}{(R_* + r)^6}\,dr = S_B \Delta n \left[\left(\frac{R_*}{T + R_*}\right)^5 - \left(\frac{R_*}{T + D + R_*}\right)^5\right] \quad (1)$$

where S_B is sensitivity to changes in the refractive index of the whole medium (bulk sensitivity) and $\Delta n = n_L - n_m$, n_m stands for the refractive index of the surrounding medium (buffer). The values of S_B and R_* were extracted from the fit of eq 1 to FDTD results (S_B = 118 nm/RIU and R_* = 70 nm for silica-coated nanodisks and S_B = 138 nm/RIU and R_* = 74.1 nm for titania-coated nanodisks). The analytical values of $\Delta\lambda_{max}$ calculated according to eq 1 are shown on Figure 3C (solid line). The trend in $\Delta\lambda_{max}$ shift as a function of separation distance is nearly linear, and the calculated $\Delta\lambda_{max}$ values are also consistent with literature reports, confirming the accuracy of our theoretical model.[30] For both substrates, the results demonstrate that, for an SLB with fixed thickness, the absolute separation distance can be directly determined from $\Delta\lambda_{max}$.

As mentioned above, it is also important to compare LSPR measurement data across substrates with different surface sensitivities. Indeed, this approach provides the basis for comparing SLB separation distances on different surfaces. In previous work, we reported that there is close agreement between the bulk and surface sensitivities of titania- and silica-coated gold nanodisk arrays.[29] This approach provided the basis to quantitatively compare $\Delta\lambda_{max}$ shifts for adsorbed vesicles on the two substrates by normalizing the $\Delta\lambda_{max}$ shifts according to the bulk refractive index sensitivities. Here, we verify that the normalization approach is applicable to spatial proximity measurements by comparing the ratio of experimentally determined bulk refractive index sensitivities (133 and 119 nm/RIU for titania- and silica-coated gold nanodisks,

DOI: 10.1021/acs.analchem.8b02222
Anal. Chem. 2018, 90, 12503−12511

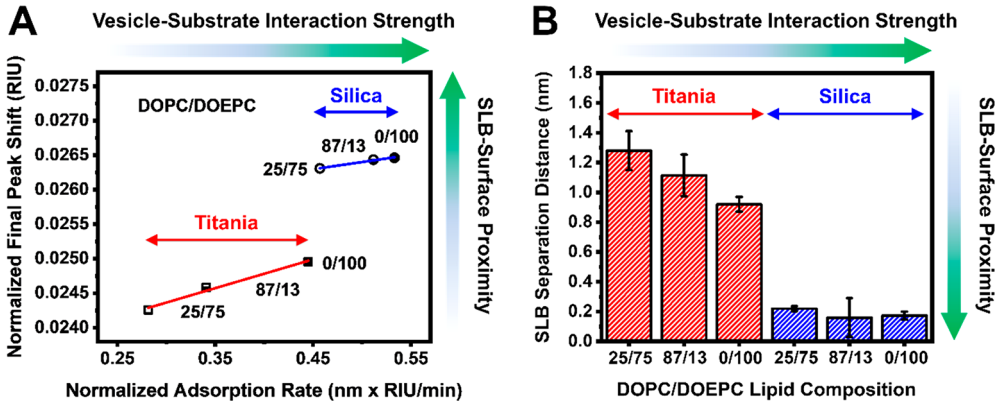

Figure 5. (A) Relationship between the normalized rate of vesicle adsorption and final LSPR measurement responses on different surfaces. (B) Comparison of absolute separation distances for SLBs on titania- and silica-coated sensor surfaces. Mean values are reported, and error bars represent the standard error (n = 3).

respectively) to the ratio of analytically calculated $\Delta\lambda_{max}$ shifts for SLBs on each substrate (cf. eq 1) across the tested range of separation distances (0−5 nm, in 0.1 nm units). Compared to the analytical calculations, it was determined that the normalization procedure resulted in a <0.4% deviation in measurement response (Table S1), and hence provides a useful approach to compare spatial proximity data across titania- and silica-coated nanodisk arrays.

LSPR Measurement Data. A prerequisite for spatial proximity measurements is the formation of a conformal, two-dimensional SLB across the sensor surface. As a first step, we therefore focused on defining appropriate lipid compositions and experimental protocols to form SLBs on titania- and silica-coated surfaces. Quartz crystal microbalance-dissipation (QCM-D) experiments identified that vesicles composed of mixtures of zwitterionic DOPC and positively charged DOEPC lipids adsorbed and ruptured spontaneously to form SLBs on both surfaces (Figure S1). It was identified that DOPC/DOEPC lipid vesicles with ≥75 mol % DOEPC lipid fraction are suitable for preparing SLBs for spatial proximity measurements. Under the experimental conditions, the oxide coatings are negatively charged, so positively charged lipid vesicles have an attractive electrostatic interaction with the sensor surface. In principle, a greater fraction of DOEPC lipids would increase electrostatic attraction and result in stronger vesicle−substrate interactions.

On the basis of the defined experimental conditions, we fabricated SLBs on titania- and silica-coated gold nanodisk arrays and evaluated the corresponding $\Delta\lambda_{max}$ shifts. The tested DOPC/DOEPC lipid compositions contained 75%, 87%, and 100% DOEPC lipid. The selected range of lipid compositions ensured successful SLB formation while maximizing possible variation in lipid−substrate interaction strength and hence SLB separation distance (as interpreted by $\Delta\lambda_{max}$ shifts). In addition, all SLBs contained a major fraction of DOEPC phospholipid and were modeled with uniform D and Δn properties. Of note, DOPC and DOEPC phospholipids are structurally similar with identical chain properties and the only difference is that DOEPC has an ethylated phosphate group.[52] Experimentally, once a baseline signal in buffer solution was established, vesicles in equivalent buffer solution were added leading to SLB formation, and final $\Delta\lambda_{max}$ shifts were recorded after a buffer washing step.

On titania surfaces, the SLB formation kinetics showed two-step adsorption behavior (Figure 4A). Initially, vesicles adsorbed and remained intact until reaching a critical surface coverage. During this initial stage, there was a constant rate of change in the LSPR signal that was controlled by the diffusion-limited rate of vesicle adsorption.[53] Once the critical coverage was reached, vesicle rupture commenced, as indicated by an increase in the rate of change in the LSPR signal. This increase denotes a rate acceleration that is attributed to continuing vesicle adsorption together with adsorbed lipid molecules rearranging to form an SLB.[21] The latter process involves the vesicle-to-bilayer structural transformation and results in adsorbed lipid molecules being, on average, closer to the sensor surface and hence in a region of higher field intensity. The final $\Delta\lambda_{max}$ shifts for SLB formation were 3.72 ± 0.04, 3.77 ± 0.04, and 3.83 ± 0.02 nm for lipid compositions containing 75, 87, and 100 mol % DOEPC lipid fractions, respectively. This finding supports that there are larger $\Delta\lambda_{max}$ shifts for SLBs with stronger lipid−substrate interactions (and hence smaller separation distances), in line with the analytical calculations and simulation results. At a quantitative level, the trend in $\Delta\lambda_{max}$ shifts supports that the difference in SLB separation distance on titania surfaces varies by around 0.4 nm for the tested compositions (cf. Figure 3C).

First-order derivative plots of the time-resolved $\Delta\lambda_{max}$ shifts further verified SLB formation kinetics (Figure 4B). For each tested lipid composition, there was a nearly constant rate of change in the LSPR signal when the surface coverage of adsorbed vesicles was low (initial adsorption stage), as indicated by a horizontal slope region in the derivative plot. The magnitude of this slope ranged from ∼35 nm/min for 25/75 mol % DOPC/DOEPC vesicles to ∼60 nm/min for 100 mol % DOEPC vesicles. In this adsorption regime, the diffusion flux of lipid vesicles contacting the sensor surface is equivalent and the difference in slope values arise from an additional contributing factor to the LSPR signal, the extent to which adsorbed vesicles undergo shape deformation. A larger slope indicates greater vesicle deformation, hence supporting the 100 mol % DOEPC vesicles are the most deformed and the trend in lipid−substrate interactions is in line with the SLB proximity data.

By contrast, SLB formation on silica surfaces occurred via a one-step process whereby vesicles adsorbed and ruptured spontaneously without requiring a critical coverage (Figure 4C). This SLB formation pathway is consistent with previous works,[30,38,54] which demonstrated the spontaneous rupture of individual, positively charged lipid vesicles on silica due to

DOI: 10.1021/acs.analchem.8b02222
Anal. Chem. 2018, 90, 12503−12511

strong lipid−substrate interactions. Interestingly, the final $\Delta\lambda_{max}$ shifts for SLB formation were around 3.15 nm for all tested compositions. Hence, within the relatively narrow range of tested lipid compositions, the results suggest that the fabricated SLBs have nearly equivalent spatial proximities on silica surfaces. First-order derivative plots support that the lipid−substrate interaction strengths are similar across the tested lipid compositions, as indicated by slopes around ∼65 nm/min in all cases (Figure 4D). On the basis of the analytical calculations and simulation results, the measurement data indicate that there is tight SLB coupling to the silica surface, with an estimated separation distance of around 0.2 nm (cf. Figure 3C). Taken together, the results demonstrate that LSPR sensing can detect minor variations in SLB spatial proximity and suggest that SLB configurations differ across titania and silica surfaces.

Comparison of Bilayer−Substrate Separation Distance. To compare LSPR measurement data across the different sensor surfaces, we normalized the data according to the corresponding bulk refractive index sensitivities as described above. The final shifts obtained for SLBs from all tested lipid compositions are reported in RI units (RIU) along with the corresponding slope magnitudes for the vesicle adsorption process (Figure 5A). The results indicate that the final $\Delta\lambda_{max}$ shifts for SLB formation are significantly larger on silica than on titania surfaces, supporting that SLBs are more tightly coupled to silica surfaces. The extent of vesicle deformation is also greater for adsorbed vesicles on silica than on titania surfaces, as indicated by larger slope magnitudes. Together, the findings support that lipid−substrate interactions are stronger on silica than on titania surfaces, and as a consequence, there is a larger separation distance between SLBs and titania surfaces than silica surfaces.

On the basis of the magnitudes of the normalized $\Delta\lambda_{max}$ shifts, we applied eq 1 in order to determine the absolute separation distance between SLBs and oxide surfaces (Figure 5B). On titania surfaces, we determined that the separation distance is around 1 nm. For 25/75 mol % DOPC/DOEPC SLBs, the separation distance was 1.28 ± 0.13 nm, whereas the separation distance was 0.92 ± 0.05 nm for 100 mol % DOEPC SLBs. Hence, the magnitude of the separation distance varied according to the lipid−substrate interaction strength. On the other hand, on silica surfaces, it was observed that the separation distance is much smaller, with values around 0.2 nm for all tested lipid compositions. These values are in line with recent simulations[55] showing that phospholipid molecules can be closely attached to silica surfaces, with an inhomogeneous molecule-thin hydration layer (≤0.4 nm). The measured values are also consistent with the separation distances (0.5−1 nm) that were reported for zwitterionic SLBs on silica surfaces, as determined by QCM-D measurements.[49,50] Of note, QCM-D is sensitive to the solvent mass of the hydration layer, and the layer thickness (i.e., the separation distance) was calculated by assuming that the density of the hydration layer is equivalent to that of bulk water. However, it is known that the properties of interfacial water are significantly different from bulk water, including higher density[56] and viscosity.[57] For this reason, the hydration layer thicknesses determined by QCM-D measurements are likely overestimates, and the actual separation distances are smaller and in the range of the LSPR measurement results.

Also, SLB compositions tested in the present work are positively charged, so the smaller separation distance is consistent with stronger lipid−substrate interactions as discussed above. Likewise, the LSPR-measured SLB separation distances in this work are consistent with past fluorescent interference contrast microscopy (FLIC) measurements, which indicated that the separation distance for a zwitterionic SLB on a silica surface is around 1.3 ± 0.2 nm (ref 58) to 1.7 ± 1.0 nm (ref 59). Of note, FLIC experiments require fluorescent labeling of the SLB, and the distribution of fluorophores between the two bilayer leaflets needs to be explicitly determined to yield accurate data.[60] As such, by directly relating the magnitude of the LSPR response to the separation distance based on first principles, the label-free LSPR measurement approach is broadly applicable, and our findings provide the first direct experimental evidence indicating that SLBs on silica surfaces are more tightly coupled than equivalent SLBs on titania surfaces.

We recall that the separation distance is largely defined by the thickness of the lubricating hydration layer that couples the SLB to the underlying solid support, and hence, the results further suggest that there is a thicker hydration layer on titania surfaces. This trend agrees well with previous reports describing how the high polarizability of titania surfaces induces a strongly attractive van der Waals force between the titania surface and contacting interfacial water molecules.[61−63] The resulting thick hydration layer on titania surfaces—arising from the buildup of adsorbed water molecules—is related to a more repulsive steric-hydration force, which decreases the overall lipid−substrate interaction strength and also explains in part why adsorbed vesicles often remain intact on titania surfaces.[64] Due to steric effects, the hydration layer also attenuates the magnitude of the attractive, but short-range, van der Waals force between lipid molecules and the titania surface.[61] On the other hand, the measured separation distances indicate that there is only a thin layer of interfacial water molecules on silica surfaces. This finding is consistent with the lower polarizability of silica surfaces, which induces a relatively weak van der Waals attractive force, and hence, there is less buildup of adsorbed water molecules. As a result, there is a weaker repulsive steric-hydration force on silica surfaces, and hence, overall lipid−substrate interactions are stronger on silica surfaces. In summary, the variation in SLB coupling to titania and silica surfaces can be understood by taking into account the close relationship between separation distance and interfacial forces in the system under consideration.

■ CONCLUSION

In this work, we have presented a nanoplasmonic ruler strategy that can be employed to comparatively measure the separation distance between SLBs and different oxide surfaces. The measurement strategy combines the highly surface-sensitive detection capabilities of LSPR sensors with an analytical model describing how the LSPR measurement response relates to the SLB separation distance. Within this scope, indirect nanoplasmonic sensing facilitated the use of oxide film-coated sensing platforms whereby embedded gold nanodisks serve as plasmonic antennas, and it was therefore possible to understand how the material properties of oxide surfaces influence SLB separation distance. In particular, the LSPR experimental approach provided the first direct evidence that there is a larger separation distance between SLBs and titania surfaces than silica surfaces. This finding agrees well with the emerging picture of how interfacial forces stabilize phospholipid assemblies on different solid supports, and the LSPR

DOI: 10.1021/acs.analchem.8b02222
Anal. Chem. 2018, 90, 12503−12511

measurement approach presents competitive advantages compared to other scattering, microscopic, and gravimetric techniques, including simple operation, high surface sensitivity, accurate quantification, and first-principles modeling. Looking forward, the nanoplasmonic ruler strategy demonstrates excellent potential for characterizing the structural properties of biomacromolecular thin films.

■ ASSOCIATED CONTENT

Supporting Information

The Supporting Information is available free of charge on the ACS Publications website at DOI: 10.1021/acs.analchem.8b02222.

Descriptions of additional methods, quantitative comparison between experimentally measured and analytically calculated responses, and SLB characterization experiments (PDF)

■ AUTHOR INFORMATION

Corresponding Author

*E-mail: njcho@ntu.edu.sg.

ORCID

Barbora Špačková: 0000-0002-8442-5641

Joshua A. Jackman: 0000-0002-1800-8102

Nam-Joon Cho: 0000-0002-8692-8955

Author Contributions

‖A.R.F. and B.S. contributed equally to this work.

Notes

The authors declare no competing financial interest.

■ ACKNOWLEDGMENTS

This work was supported by the National Research Foundation of Singapore through a Proof-of-Concept Grant (NRF2015NRF-POC0001-19) and the Czech Science Foundation (GBP205/12/G118) as well as through the Center for Precision Biology at Nanyang Technological University. Additional support was provided by the Creative Materials Discovery Program through the National Research Foundation of Korea (NRF) funded by the Ministry of Science, ICT and Future Planning (NRF-2016M3D1A1024098).

■ REFERENCES

(1) Dahlin, A. B.; Wittenberg, N. J.; Höök, F.; Oh, S.-H. *Nanophotonics* **2013**, *2*, 83−101.
(2) Estevez, M.-C.; Otte, M. A.; Sepulveda, B.; Lechuga, L. M. *Anal. Chim. Acta* **2014**, *806*, 55−73.
(3) Lopez, G. A.; Estevez, M.-C.; Soler, M.; Lechuga, L. M. *Nanophotonics* **2017**, *6*, 123−136.
(4) Jackman, J. A.; Ferhan, A. R.; Cho, N.-J. *Chem. Soc. Rev.* **2017**, *46*, 3615−3660.
(5) Sannomiya, T.; Scholder, O.; Jefimovs, K.; Hafner, C.; Dahlin, A. B. *Small* **2011**, *7*, 1653−1663.
(6) Stockman, M. I. *Science* **2015**, *348*, 287−288.
(7) Mazzotta, F.; Johnson, T. W.; Dahlin, A. B.; Shaver, J.; Oh, S.-H.; Höök, F. *ACS Photonics* **2015**, *2*, 256−262.
(8) Špačková, B.; Wrobel, P.; Bocková, M.; Homola, J. *Proc. IEEE* **2016**, *104*, 2380−2408.
(9) Mayer, K. M.; Hafner, J. H. *Chem. Rev.* **2011**, *111*, 3828−3857.
(10) Willets, K. A.; Van Duyne, R. P. *Annu. Rev. Phys. Chem.* **2007**, *58*, 267−297.
(11) Unser, S.; Bruzas, I.; He, J.; Sagle, L. *Sensors* **2015**, *15*, 15684−15716.
(12) Anker, J. N.; Hall, W. P.; Lyandres, O.; Shah, N. C.; Zhao, J.; Van Duyne, R. P. *Nat. Mater.* **2008**, *7*, 442.
(13) Langhammer, C.; Larsson, E. M.; Kasemo, B.; Zoric, I. *Nano Lett.* **2010**, *10*, 3529−3538.
(14) Larsson, E. M.; Syrenova, S.; Langhammer, C. *Nanophotonics* **2012**, *1*, 249−266.
(15) Russo, G.; Witos, J.; Rantamäki, A. H.; Wiedmer, S. K. *Biochim. Biophys. Acta, Biomembr.* **2017**, *1859*, 2361−2372.
(16) Witos, J.; Russo, G.; Ruokonen, S.-K.; Wiedmer, S. K. *Langmuir* **2017**, *33*, 1066−1076.
(17) Duša, F.; Chen, W.; Witos, J.; Wiedmer, S. K. *Langmuir* **2018**, *34*, 5889−5900.
(18) Jackman, J. A.; Ferhan, A. R.; Yoon, B. K.; Park, J. H.; Zhdanov, V. P.; Cho, N.-J. *Anal. Chem.* **2017**, *89*, 12976−12983.
(19) Zan, G. H.; Jackman, J. A.; Kim, S. O.; Cho, N. *Small* **2014**, *10*, 4828−4832.
(20) Czolkos, I.; Jesorka, A.; Orwar, O. *Soft Matter* **2011**, *7*, 4562−4576.
(21) Jonsson, M. P.; Jönsson, P.; Dahlin, A. B.; Höök, F. *Nano Lett.* **2007**, *7*, 3462−3468.
(22) Larsson, E. M.; Edvardsson, M. E.; Langhammer, C.; Zorić, I.; Kasemo, B. *Rev. Sci. Instrum.* **2009**, *80*, 125105.
(23) Jackman, J. A.; Zhdanov, V. P.; Cho, N.-J. *Langmuir* **2014**, *30*, 9494−9503.
(24) Oh, E.; Jackman, J. A.; Yorulmaz, S.; Zhdanov, V. P.; Lee, H.; Cho, N.-J. *Langmuir* **2015**, *31*, 771−781.
(25) Dacic, M.; Jackman, J. A.; Yorulmaz, S.; Zhdanov, V. P.; Kasemo, B.; Cho, N.-J. *Langmuir* **2016**, *32*, 6486−6495.
(26) Kojima, T. *Anal. Chem.* **2017**, *89*, 13596−13602.
(27) Seifert, U.; Lipowsky, R. *Phys. Rev. A: At., Mol., Opt. Phys.* **1990**, *42*, 4768.
(28) Lipowsky, R.; Seifert, U. *Mol. Cryst. Liq. Cryst.* **1991**, *202*, 17−25.
(29) Jackman, J. A.; Špačková, B.; Linardy, E.; Kim, M. C.; Yoon, B. K.; Homola, J.; Cho, N.-J. *Chem. Commun.* **2016**, *52*, 76−79.
(30) Ferhan, A. R.; Jackman, J. A.; Cho, N.-J. *Anal. Chem.* **2017**, *89*, 4301−4308.
(31) Wiegand, G.; Arribas-Layton, N.; Hillebrandt, H.; Sackmann, E.; Wagner, P. *J. Phys. Chem. B* **2002**, *106*, 4245−4254.
(32) Seeger, H. M.; Cerbo, A. D.; Alessandrini, A.; Facci, P. *J. Phys. Chem. B* **2010**, *114*, 8926−8933.
(33) Wargenau, A.; Tufenkji, N. *Anal. Chem.* **2014**, *86*, 8017−8020.
(34) Hasan, I. Y.; Mechler, A. *Anal. Chem.* **2017**, *89*, 1855−1862.
(35) Mager, M. D.; Almquist, B.; Melosh, N. A. *Langmuir* **2008**, *24*, 12734−12737.
(36) Venkatesan, B. M.; Polans, J.; Comer, J.; Sridhar, S.; Wendell, D.; Aksimentiev, A.; Bashir, R. *Biomed. Microdevices* **2011**, *13*, 671−682.
(37) Jiménez, C.; Perriere, J.; Vickridge, I.; Enard, J. P.; Albella, J. M. *Surf. Coat. Technol.* **1991**, *45*, 147−154.
(38) Ferhan, A.; Ma, G.; Jackman, J.; Sut, T.; Park, J.; Cho, N.-J. *Sensors* **2017**, *17*, 1484.
(39) Dahlin, A. B.; Tegenfeldt, J. O.; Höök, F. *Anal. Chem.* **2006**, *78*, 4416−4423.
(40) Johnson, P. B.; Christy, R. W. *Phys. Rev. B* **1972**, *6*, 4370−4379.
(41) Fredriksson, H.; Alaverdyan, Y.; Dmitriev, A.; Langhammer, C.; Sutherland, D. S.; Zäch, M.; Kasemo, B. *Adv. Mater.* **2007**, *19*, 4297−4302.
(42) Larsson, E. M.; Millet, J.; Gustafsson, S.; Skoglundh, M.; Zhdanov, V. P.; Langhammer, C. *ACS Catal.* **2012**, *2*, 238−245.
(43) Grigorchuk, N. I. *J. Phys. Chem. C* **2012**, *116*, 23704−23712.
(44) Myroshnychenko, V.; Rodriguez-Fernandez, J.; Pastoriza-Santos, I.; Funston, A. M.; Novo, C.; Mulvaney, P.; Liz-Marzan, L. M.; Garcia de Abajo, F. *Chem. Soc. Rev.* **2008**, *37*, 1792−1805.
(45) Chou, L.-W.; Near, R. D.; Boyuk, D. S.; Filler, M. A. *J. Phys. Chem. C* **2014**, *118*, 5494−5500.
(46) Kučerka, N.; Tristram-Nagle, S.; Nagle, J. F. *J. Membr. Biol.* **2006**, *208*, 193−202.

DOI: 10.1021/acs.analchem.8b02222
Anal. Chem. 2018, 90, 12503−12511

(47) Drolle, E.; Kučerka, N.; Hoopes, M.; Choi, Y.; Katsaras, J.; Karttunen, M.; Leonenko, Z. *Biochim. Biophys. Acta, Biomembr.* **2013**, *1828*, 2247−2254.
(48) Mashaghi, A.; Swann, M.; Popplewell, J.; Textor, M.; Reimhult, E. *Anal. Chem.* **2008**, *80*, 3666−3676.
(49) Anderson, T. H.; Min, Y.; Weirich, K. L.; Zeng, H.; Fygenson, D.; Israelachvili, J. N. *Langmuir* **2009**, *25*, 6997−7005.
(50) Zwang, T. J.; Fletcher, W. R.; Lane, T. J.; Johal, M. S. *Langmuir* **2010**, *26*, 4598−4601.
(51) Li, A. R.; Lim, X. Y.; Guo, L.; Li, S. Z. *Nanotechnology* **2018**, *29*, 165501.
(52) MacDonald, R. C.; Gorbonos, A.; Momsen, M. M.; Brockman, H. L. *Langmuir* **2006**, *22*, 2770−2779.
(53) Zhdanov, V.; Keller, C.; Glasmästar, K.; Kasemo, B. *J. Chem. Phys.* **2000**, *112*, 900−909.
(54) Cho, N.-J.; Frank, C. W.; Kasemo, B.; Höök, F. *Nat. Protoc.* **2010**, *5*, 1096.
(55) Vishnyakov, A.; Li, T.; Neimark, A. V. *Langmuir* **2017**, *33*, 13148−13156.
(56) Argyris, D.; Tummala, N. R.; Striolo, A.; Cole, D. R. *J. Phys. Chem. C* **2008**, *112*, 13587−13599.
(57) Schoch, R. L.; Barel, I.; Brown, F. L.; Haran, G. *J. Chem. Phys.* **2018**, *148*, 123333.
(58) Ajo-Franklin, C. M.; Yoshina-Ishii, C.; Boxer, S. G. *Langmuir* **2005**, *21*, 4976−4983.
(59) Kiessling, V.; Tamm, L. K. *Biophys. J.* **2003**, *84*, 408−418.
(60) Lambacher, A.; Fromherz, P. *Appl. Phys. A: Mater. Sci. Process.* **1996**, *63*, 207−216.
(61) Zhdanov, V.; Kasemo, B. *Langmuir* **2001**, *17*, 5407−5409.
(62) Reimhult, E.; Höök, F.; Kasemo, B. *Langmuir* **2003**, *19*, 1681−1691.
(63) Tero, R.; Ujihara, T.; Urisu, T. *Langmuir* **2008**, *24*, 11567−11576.
(64) Jackman, J. A.; Tabaei, S. R.; Zhao, Z.; Yorulmaz, S.; Cho, N.-J. *ACS Appl. Mater. Interfaces* **2015**, *7*, 959−968.

DOI: 10.1021/acs.analchem.8b02222
Anal. Chem. 2018, 90, 12503−12511